



## Lateral dynamic identification of a hatchback vehicle

Rafael Rodrigues da Silva<sup>1</sup>, Reurison Silva Rodrigues<sup>2</sup>, André Murilo<sup>3</sup>, Helon Vicente Hultmann Ayala<sup>4</sup>, Evandro Leonardo Silva Teixeira<sup>1</sup>

<sup>1</sup>*Dept. of Automotive Engineering, University of Brasília (UnB)  
Brasília, Brasil*

*rafael.rodrigues@unb.br*

<sup>2</sup>*Instituto Tecnológico de Buenos Aires*

*Buenos Aires, Argentina*

*rsilva@itba.edu.ar*

<sup>3</sup>*Universidade Federal de Lavras*

*Minas Gerais, Brasil*

*andremurilo@gmail.com*

<sup>4</sup>*PUC RIO*

*Rio de Janeiro, Brasil*

*helon@puc-rio.br*

### Abstract

Vehicle dynamics identification plays a critical role in understanding and modeling the complex behavior of vehicles during maneuvers and it is fundamental to the design of Electronic Stability Control (ESC) once a mathematical vehicle model needs to be embedded into the brake ECU to calculate the desired yaw rate. This calculated value is subsequently compared to the measured yaw rate to define ESC actuation during the maneuver. This paper discusses linear methods for vehicle dynamics system identification, encompassing both model-based and data-driven approaches. Model-based methods rely on physical principles and mathematical models to describe the dynamics, while data-driven methods leverage experimental data to identify system parameters and behaviors. The focus of this study is the identification of a 2-DOF (Degree-of-Freedom) vehicle model based on real data acquired from a hatchback vehicle. The hatchback vehicle was instrumented and several maneuvers were performed on a test track to generate data for identification purposes. Furthermore, different speeds of the vehicle were considered for the identification, followed by a comparison between all the identified models.

**Keywords:** System Identification, Vehicle Dynamics, Data Driven

## 1 Introduction

A considerable portion of vehicle accidents can be attributed to human errors. Factors such as delayed reactions, limited visibility and driver drowsiness can increase the risk of accidents [1]. To address this issue, modern cars are equipped with active driver-assist functions that aim to reduce the number of accidents or mitigate their severity [2].

Electronic Stability Control (ESC) is one of the most significant active vehicle systems and the main goal is to maintain the lateral control of the vehicle in emergency conditions [3]. The ESC system can reduce crashes and injuries when compared with non-ESC-equipped vehicles [4]. These are reasons why ESC system has been more and more used as a standard configuration for automotive manufacturers and has been widely studied by research institutions.

The ESC plays a crucial role in enhancing vehicle safety and stability during dynamic maneuvers. By utilizing different sensors, the system continuously monitors the vehicle's actual state, mainly yaw rate and side slip angle. These measurements are then compared with the desired path planning, which is inferred from the driver's actions, such as steering inputs and then the control action is performed in order to keep the stability of the vehicle.

By dynamically adjusting the brake pressure on individual wheels, the ESC effectively assists the driver in maintaining control and stability, especially in challenging road conditions or sudden maneuvers. This intervention can prevent potential skidding, loss of control, and potential accidents, making the Electronic Stability Control system a valuable safety feature in modern vehicles. [5] [6].

The calculation of the desired yaw rate, which is later compared to the actual vehicle state, is performed by the brake Electronic Control Unity (ECU) based on the driver's input over a reference vehicle model[7]. In this sense, the vehicle model plays an important part in the ESC control strategy once it generates the desired yaw rate. Furthermore, the reference model is also used for the development of model-based control strategies such as Model Predictive Control (MPC), Linear Quadratic Regulator (LQR) and Linear parameter-varying control (LPV). A number of studies have proposed reference vehicle models for control applications. Below, an overview of various works is provided

In [8], the authors put forward a comprehensive and insightful proposal of a 2-DOF bicycle model, which serves as a reference vehicle model for the design of an Electronic Stability Control (ESC) system. The choice of this particular model stems from its ability to effectively capture the essential dynamics of a typical vehicle's motion. In [9], a 3-DOF yaw plane model is developed for ESC control, while a 2-DOF bicycle model incorporating tires is adopted for controlling the Active Front Steer (AFS). Regarding the usage of robust controllers, a 2-DOF vehicle model is designed in order to provide the yaw reference for the Model Predictive Controller (MPC) [10]. Despite the widespread use of the 2-DOF as a reference vehicle in numerous studies, this model cannot describe the car's dynamics in every situation, as it has some limitations, particularly under extreme conditions [10].

Another approach for modeling vehicle dynamics is through system identification. This method involves utilizing vehicle data as input/output to develop a model that accurately represents the behavior of the system under examination. System identification is a powerful technique that enables engineers and researchers to analyze complex systems, such as vehicles, without the need for explicit knowledge of their underlying physical principles. Several works implement system identification for modeling vehicle dynamics behavior.

In [11] the identification of a 6x6 military vehicle model is performed using the CONTSID (CONTinuous-time System IDentification) toolbox[12]. A double lane change maneuver is executed to gather data directly from the vehicle. The identification resulted in a specific transfer function for each vehicle's speed. A non-linear model-based observer is implemented in [13]. The paper presents the usage of an augmented Extended Kalman filter for the online identification of tire cornering stiffness using onboard sensors. The identified model is used to improve the performance of the active control system.

In this current study, a continuous-time model identification of a hatchback vehicle is performed. The vehicle was instrumented with sensors and a series of maneuvers were executed on the test track. Subsequently, the acquired data is used for model identification purposes. The analysis of the transfer function between yaw rate and wheel steering angle, examining how varying speeds impact the identification process. Furthermore, a linear identification approach is employed and their outcomes are discussed. Consequently, the main contribution of this paper resides in the application of linear identification technique to a hatchback vehicle, along with an investigation into the influence of speed on these models.

This paper is organized in the following order. The details of the vehicle model are in Section II. In Section III, a linear identification technique is designed. The methodology for the identification procedure is described in IV. The results are given in Section V and the paper is concluded in the discussion in Section VI.

## 2 Vehicle Dynamics Modeling

A mathematical model is one of the main approaches to representing a complex dynamic system. The vehicle mathematical model can be described with different DOF based on the number of dynamics considered. A simple way of representing a vehicle's motion is the bicycle model, in this model the steering system, suspension system, aerodynamic, pitch, and roll movement are neglected and the vehicle moves on a rigid surface. The model has 2-DOF, translational in the lateral direction and rotational motion of yaw such as shown in Figure 1.

In this model,  $R$  is the radius of the turn,  $L = a + b$  is the wheelbase,  $\beta = \arctan(v/u) \approx v/u$  (for small angles) is the side-slip angle at CG,  $u$  the longitudinal speed,  $\alpha_f$  and  $\alpha_r$  are the wheel sleep angle of the front and rear wheels respectively,  $v$  the lateral speed and the yaw rate  $r = \dot{\psi}$ . Considering the geometrical relationship between the terms in Figure 1, we obtain:

$$\alpha_f = \delta_f - \frac{v + ar}{u} \quad (1)$$

$$\alpha_r = -\frac{v - br}{u} \quad (2)$$

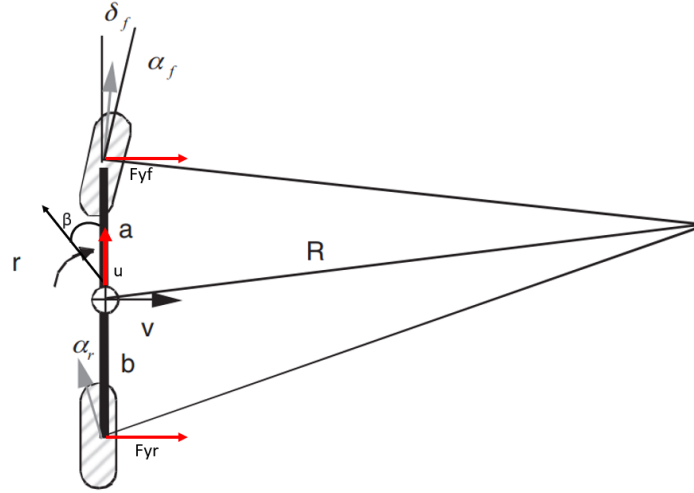


Figure 1. Schematic of bicycle model [3]

Considering that the instantaneous speed tangent to the path at the CG is  $u = rR$ , one can obtain

$$\alpha_f - \alpha_r = \delta_f - \frac{L}{R} \quad (3)$$

$$\delta_f = \frac{L}{R} + \alpha_f - \alpha_r \quad (4)$$

These equations can be subdivided into two parts: the static part ( $L/R$ ) and the dynamic part which represents the difference between the front and rear tire-slip angles. In the case where the front tire slip angle is larger than the rear tire slip angle, this situation is referred to as understeer. On the other hand, if the rear tire slip angle is larger than the front tire slip angle, it means an oversteer situation. When both slip angles are equal, this represents a neutral condition. Applying the second Newton's Law for the direction  $y$  of the movement, one obtains:

$$F_{yf} + F_{yr} = ma_y \quad (5)$$

Taking into account the centripetal acceleration component, the lateral acceleration transforms into  $a_y = \dot{v} + ur$ . Thus,

$$F_{yf} + F_{yr} = ma_y = m(\dot{v} + ur) \quad (6)$$

where equation 6 is the first equation of state for the force representing the first degree of freedom and the second equation for the moment is 8. By introducing an external stabilizing torque  $M_{esc}$  computed by the ESC algorithm, the following arrangement is achieved:

$$F_{yf} + F_{yr} = mu\dot{\psi} + m\dot{v} \quad (7)$$

$$M_{esc} + aF_{yf} - bF_{yr} = I_z\ddot{\psi} \quad (8)$$

Equations 7 and 8 can be written in a nonlinear state-space format:

$$\dot{x} = -E^{-1}Fx + E^{-1}Gu + E^{-1}Hw \quad (9)$$

where  $x(t) = [v, \psi]^T$  is the state vector,  $u = M_{esc}$  is the controlled input signal and  $w = [F_{yf}, F_{yr}]^T$  an external input signal acting on the system. The matrices  $E$ ,  $F$ ,  $G$  and  $H$  are:

$$E = \begin{bmatrix} m & 0 \\ 0 & I_z \end{bmatrix} \quad F = \begin{bmatrix} 0 & mu \\ 0 & 0 \end{bmatrix} \quad G = \begin{bmatrix} 0 \\ 1 \end{bmatrix} \quad H = \begin{bmatrix} 1 & 1 \\ a & -b \end{bmatrix} \quad (10)$$

### 3 Continuous-time Model Identification Problem

The continuous-time (CT) system identification problem consists of obtaining a continuous model from sampled data. Garnier et al. [14] describes two methods in time domain for accomplishing this task. The indirect approach uses experimental data to obtain a discrete model and then performs a continuous approximation, for example using *ZOH* (Zero-Order Hold). The second method called direct, does not need to obtain an intermediate discrete model to approximate a continuous model. Given that the experimental data of a model has an inherently discrete nature, it is possible to initially conclude that a discrete-time (DT) identification is the most recommended technique. But, one of the main advantages of CT identification is that they are more intuitive because the model can be interpreted in physically meaningful terms [15], and these models are not restricted to the same sample time used to obtain the experimental data [14]. The general problem of continuous-time system identification can be expressed initially through the representation in differential equations of a Linear Time-Invariant (LTI) system [14]:

$$\begin{aligned} & y^{(n)}(t) + a_1 y^{(n-1)}(t) + \dots + a_{n-1} \dot{y}(t) + a_n y(t) \\ & = b_0 u^{(m)}(t) + b_1 u^{(m-1)}(t) + \dots + b_{m-1} \dot{u}(t) + b_m u(t) + v(t) \end{aligned} \quad (11)$$

where  $y^{(n)}(t)$  is the  $n$ -th time derivative of the input signal and  $u^{(m)}(t)$  the  $m$ -th time derivative of the model output signal and  $v(t)$  represents measurement error. Writing equation 11 in the time-domain differential operator form:

$$y = \frac{B(p)}{A(p)} u(t) + \xi(t) \quad (12)$$

$$\xi(t) = \frac{1}{A(p)} v(t) \quad (13)$$

$$A(p) = p^n + a_1 p^{n-1} + \dots + a_{n-1} p + a_n \quad (14)$$

$$B(p) = b_0 p^m + b_1 p^{m-1} + \dots + b_{m-1} p + b_m \quad (15)$$

where  $p^n$  is the  $n$ -th order time differential operator  $d^n/dt^n$ . At any time instant  $t = t_k$  equation 12 can be written in linear regression form:

$$y^{(n)}(t_k) = \phi^T(t_k) \theta + v(t_k) \quad (16)$$

$$\phi^T(t_k) = [-y^{(n-1)}(t_k) \dots - y(t_k) u^{(m)}(t_k) \dots u(t_k)] \quad (17)$$

$$\theta^T = [a_1 \dots a_n \ b_0 \dots b_m] \quad (18)$$

To obtain the optimized vector of unknowns  $\theta$ , it is necessary to solve the following optimization problem:

$$\hat{\theta} = \arg \min_{\theta} \frac{1}{N} \sum_{k=1}^N l(\epsilon_f(t_k, \theta)) \quad (19)$$

$$\epsilon_f(t_k, \theta) = F(\bullet)(y(t_k) - \hat{y}(t_k, \theta)), \quad k \in 1, \dots, N \quad (20)$$

$$\hat{y}(t_k, \theta) = g(\theta, Z^{k-1}) \quad (21)$$

where  $\hat{y}(t_k, \theta)$  is the system predictor, dependent on a unknown parameter vector  $\theta$  and past data  $Z^{k-1}$ . The function  $F(\bullet)$  is the differential operator when CT case is assumed and  $l(\epsilon_f(t_k, \theta))$  a scalar-valued positive function. The dependence of the regression vector  $\phi^T(t_k)$  on the time derivatives of  $y^{(i)}$ ,  $u^{(j)}$ , where  $i \in \{1, \dots, n\}$  and  $j \in \{1, \dots, m\}$  poses a problem because these derivatives normally are not measured. The use of methods like RIVC (Refined Instrumental Variable) for CT systems [16] can be used to overcome this limitation. This method is well implemented in CONTSID, a MATLAB *toolbox* specifically designed for CT system identification, through the function *tfrivc*.

### 4 Experimental Data

The experimental data of steering wheel angle  $\delta_f$  and yaw rate  $\dot{\psi}$  were obtained from the hatchback vehicle by performing the Moose Test, a maneuver without braking to evade a suddenly appearing obstacle [17]. Figure 2 shows a set of data obtained experimentally from the vehicle under study.

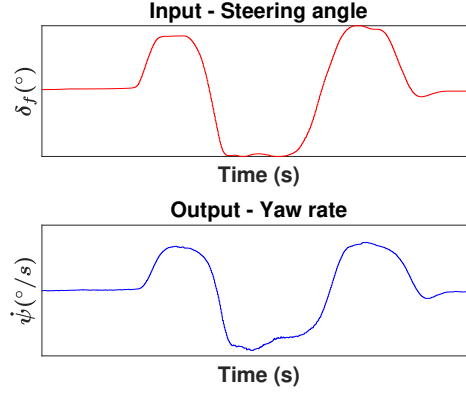


Figure 2. Input/Output experimental data obtained from Moose test.

The red line graph represents the vehicle input signal, i.e., steering angle  $\delta_f$  and the blue line graph represents the yaw rate output data  $\dot{\psi}$ , measured on a fixed coordinate axis on the vehicle body. The data were obtained at a sampling rate of 500 Hz. From the experimental data presented, it is possible to relate  $\delta_f$  and  $\dot{\psi}$  into a continuous transfer function in the complex variable  $s$  as:

$$\frac{\dot{\psi}(s)}{\delta_f(s)} = \frac{N(s)}{D(s)} = K \frac{\prod_{i=1}^{n_z} (s + z_i)}{\prod_{i=1}^{n_p} (s + p_i)} \quad (22)$$

We define  $\deg(N(s))$  and  $\deg(D(s))$  as the degree of the transfer function numerator and denominator, respectively. It is important to mention that in the experiments the following restriction is imposed  $\deg(N(s)) < \deg(D(s))$ , in order to allow only the identification of strictly proper transfer functions. This is consistent with the characteristic that real physical systems do have finite bandwidth. The values  $n_z$  and  $n_p$  are the number of zeros and poles of the transfer function, respectively. These are the free-parameters that can be chosen in the CT system identification.

## 5 Results

Different models were identified for the following longitudinal velocities: 55, 59, 58, 60, 62 and 64 km/h. Once the models were identified, validation was performed using a different set of maneuvers. In this case, a Sine With Dwell (SWD) with a longitudinal constant velocity of 80 km/h, turning initially to the right. This contrasts with the original Moose test which is performed by turning the steering wheel initially to the left, as can be seen in Figure 2. The SWD maneuver consists of a constant steering wheel sine wave with a specific dwell time at its second peak. It has been shown in [18] that SWD is often used to certify stability control systems on light vehicles.

Regarding the nonlinear state-space equation (9), is made the assumption that the order of the system is 2. Thus to accommodate this information into the identified linear transfer function (22), and also considering only strictly proper functions, it is chosen :  $n_z = 1$  and  $n_p = 2$ . Results obtained in the validation step are shown in Figure 3.

These results can be summarized in the Table 1 in terms of poles and zero locations, FIT to the original data and the multiple correlation coefficient  $R^2$ , both define as:

$$FIT = 100 \times \left( 1 - \frac{\|y(t) - \hat{y}(t)\|_2}{\|y(t) - \bar{y}(t)\|_2} \right) \quad (23)$$

$$R^2 = 1 - \frac{\sum_{t=1}^N [\xi(t)]^2}{\sum_{t=1}^N [y(t) - \bar{y}(t)]^2} \quad (24)$$

where  $\xi(t) = y(t) - \hat{y}(t)$  is the residual, or the difference between the real output from the model  $y(t)$  and  $\hat{y}(t)$  the predictions obtained with the identified model. The value  $\bar{y}(t)$  is the average value of the sequence  $y(t)$ .

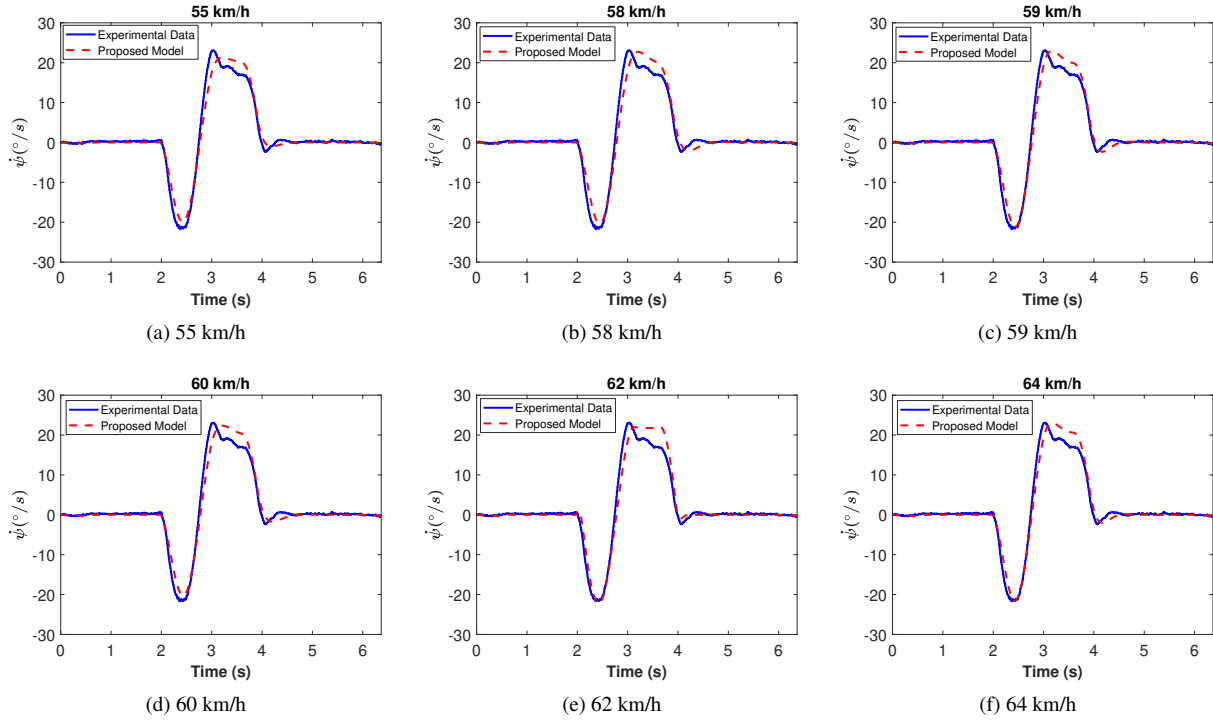


Figure 3. Results from model validation of identified CT systems for different longitudinal velocities.

Longitudinal Velocity (km/h)	Poles	Zero	K	FIT (%)	$R^2$
55	$-6.1850 \pm 5.2015i$	-8.756	1.7052	94.80	0.9668
58	$-4.4365 \pm 5.0860i$	-7.761	1.3223	80.93	0.9566
59	$-4.6725 \pm 6.2055i$	-10.67	1.2937	91.19	0.9708
60	$-4.9400 \pm 4.5537i$	-6.437	1.597	90.47	0.9626
62	$-13.7700 \pm 16.6999i$	+23.7	4.8896	90.03	0.9550
64	$-5.1450 \pm 6.5161i$	-12.48	1.3037	89.91	0.9682

Table 1. Poles and Zero locations from of identified CT systems for different forward velocities.

From Table 1 it is possible to see that all the identified models are stable, i.e.,  $\Re(p_i) < 0$ . It is worth mentioning that the identified dynamic for 62 km/h is a non-minimum phase system, presenting a zero in the right half complex plane. Although this not compromises the stability, it could impose an upper limit in terms of bandwidth achieved by a possible controller. For the sake of comparison, when CT identification is performed with  $n_p = 3$ ,  $n_z = 1$ , and focusing only in FIT and  $R^2$  results are summarized in Table 2. Results from the tables 1 and 2, shows that the assumption of lateral dynamics as a 2nd order transfer function is a good approximation for the nonlinear original model 9. It is possible to do a more exhaustive search for other combinations of  $n_p$  and  $n_z$  which could increase the FIT and  $R^2$ , but to obtain a model of greater order signifies obtain a more complicate model when considering the design of controllers or state estimators.

	55	58	59	60	62	64
<b>FIT (%)</b>	94.74	77.39	91.10	88.19	48.96	82.15
<b><math>R^2</math></b>	0.96	0.94	0.97	0.94	0.68	0.94

Table 2. CT identification, when  $n_p = 3$  and  $n_z = 1$ .

## 6 Conclusions and Future Work

A continuous-time (CT) system identification for the lateral dynamics of a hatchback vehicle has been performed. The vehicle was instrumented and a set of maneuvers were executed on a test track. The resulting data is then employed to execute the identification methods. Results showed that identified transfer functions of 2<sup>nd</sup> order offered a good approximation for the experimental data. Once these identified models are linear then it is possible to treat them with the usual linear framework tools for controller synthesis. The multiple correlation coefficient showed a good level of correlation for the different speeds. Thus, the obtained transfer function can serve as a suitable representation of the reference vehicle model for calculating the ideal yaw rate within the brake system ECU, as well as a model for designing a model-based controller. Suggestions for future works include: performing a LPV system identification, using the longitudinal velocity as a variable parameter. The use of a more diverse set of maneuvers to improve the validation of the identified system, and finally, in the base of the actual models, design and implementation of a controller directly in the ECU.

## References

- [1] R. H. Patel, J. Härrä, and C. Bonnet. A collision mitigation strategy for intelligent vehicles to compensate for human factors affecting manually driven vehicles. In *2017 IEEE 20th International Conference on Intelligent Transportation Systems (ITSC)*, pp. 114–119, 2017.
- [2] D. Shin, S. Woo, and M. Park. Rollover index for rollover mitigation function of intelligent commercial vehicle's electronic stability control. *Electronics*, vol. 10, n. 21, 2021.
- [3] A. G. Ulsoy, H. Peng, and M. Çakmakci. *Automotive control systems*. Cambridge University Press, 2012.
- [4] T. Koisaari, T. Kari, T. Vahlberg, N. Sihvola, and T. Tervo. Crash risk of esc-fitted passenger cars. *Traffic Injury Prevention*, vol. 20, n. 3, pp. 325–331, 2019.
- [5] L. Wei, X. Wang, L. Li, Z. Fan, R. Dou, and J. Lin. T-s fuzzy model predictive control for vehicle yaw stability in nonlinear region. *IEEE Transactions on Vehicular Technology*, vol. 70, n. 8, pp. 7536–7546, 2021.
- [6] A. Tahouni, M. Mirzaei, and B. Najjari. Novel constrained nonlinear control of vehicle dynamics using integrated active torque vectoring and electronic stability control. *IEEE Transactions on Vehicular Technology*, vol. 68, n. 10, pp. 9564–9572, 2019.
- [7] B. Gao, W. Tao, H. Chu, M. Tian, and H. Chen. A reference vehicle model applied to electronic stability control (esc) system. In *2017 36th Chinese Control Conference (CCC)*, pp. 9436–9441, 2017.
- [8] J. Guo, L. Chu, F. Zhou, and L. Cao. Integrated control of variable torque distribution and electronic stability program based on slip angle phase. In *Proceedings of 2011 International Conference on Electronic Mechanical Engineering and Information Technology*, volume 7, pp. 3777–3780, 2011.
- [9] S. Kolte, A. K. Srinivasan, and A. Srikrishna. Development of decentralized integrated chassis control for vehicle stability in limit handling. *SAE International Journal of Vehicle Dynamics, Stability, and NVH*, vol. 1, n. 2016-01-8106, pp. 1–10, 2016.
- [10] Y. He, J. Ma, X. Zhao, R. Song, X. Liu, and L. Wang. Coordinated stability control strategy for intelligent electric vehicles using vague set theory. *Mathematical Problems in Engineering*, vol. 2020, 2020.
- [11] C. L. Pereira, de D. H. B. Sousa, and H. V. H. Ayala. Three-axle vehicle lateral dynamics identification using double lane change maneuvers data. In *2021 29th Mediterranean Conference on Control and Automation (MED)*, pp. 910–915, 2021.
- [12] H. Garnier and M. Gilson. Consid: a matlab toolbox for standard and advanced identification of black-box continuous-time models. *IFAC-PapersOnLine*, vol. 51, n. 15, pp. 688–693, 2018.
- [13] G. Reina and A. Messina. Vehicle dynamics estimation via augmented extended kalman filtering. *Measurement*, vol. 133, pp. 383–395, 2019.
- [14] H. Garnier, L. Wang, and P. C. Young. Direct identification of continuous-time models from sampled data: Issues, basic solutions and relevance. In *Identification of continuous-time models from sampled data*, pp. 1–29. Springer, 2008.
- [15] H. Garnier. Direct continuous-time approaches to system identification. overview and benefits for practical applications. *European Journal of control*, vol. 24, pp. 50–62, 2015.
- [16] R. A. González, C. R. Rojas, S. Pan, and J. S. Welsh. Theoretical and practical aspects of the convergence of the srvc estimator for over-parameterized models. *Automatica*, vol. 142, pp. 110355, 2022.
- [17] J. J. Breuer. Analysis of driver-vehicle-interactions in an evasive manoeuvre-results of "moose test" studies. In *Proc. 16th ESV Conf., Paper*, number 98-S2, 1998.
- [18] F. Bruzelius. A theoretical justification of the sine with dwell manoeuvre. *Vehicle System Dynamics*, vol. 53, n. 4, pp. 493–505, 2015.